HEFAT2011

8th International Conference on Heat Transfer, Fluid Mechanics and Thermodynamics

11 – 13 July 2011

Pointe Aux Piments, Mauritius

FLUID DYNAMICS AROUND TWIN CYLINDERS AND INTERACTIONS

Md. Mahbub Alam* and Meyer, J.P.

*Author for correspondence

Department of Mechanical and Aeronautical Engineering

University of Pretoria

Pretoria 0002, South Africa

*Email: alam.mahbub@up.ac.za; alamm28@yahoo.com

ABSTRACT

Multiple cylindrical structures are widely seen in engineering. Flow interference between the structures leads to a very high fluctuating forces, structural vibrations, acoustic noise, or resonance, which in some cases can trigger failure. Recently circular pins in various arrays have been using as fins to enhance the cooling effect. While the enhancement is directly connected to nature of flow around the pins, no much is known of physics of flow around the pins. The knowledge of flow around two cylinders is insightful for understanding the flow around an array of cylinders/pins. This paper presents results of an experimental investigation into interactions between flowing fluid and a cylinder that is neighbored by another cylinder of the same diameter. Strouhal number (*St*), time-mean and fluctuating forces on and flow structures around the cylinder are investigated while the gap-spacing ratio *T/D* is varied from 0.1 to 5 and the attack angle α from 0° to 180° where *T* is the gap width between the cylinders, and *D* is the diameter of a cylinder. A flow visualisation test was conducted to observe flow structures around the cylinders. Based on forces, *St*, flow structures and fluid-cylinder interaction mechanisms, 19 distinct flow categories in the ranges of α and *T/D* are observed, including one quadristable flow, three tristable flows and four bistable flows. The quadristable, tristable and bistable flows ensue from instabilities of the gap flow, shear layers, vortices, separation bubbles and wakes, engendering a strong jump/drop in forces and *St* of the cylinders. Six different interaction mechanisms are observed, namely interaction between boundary layer and cylinder, shear layer/wake and cylinder, shear layer and shear layer, vortex and cylinder, vortex and shear layer, and vortex and vortex. While the interaction between vortex and cylinder results in a very high fluctuating drag, that between vortex and shear layer results in a high fluctuating lift. On the other hand, the interaction between shear layer/wake and cylinder suppresses mean and fluctuating forces as well as weakens flow unsteadiness for stationary cylinders but may cause violent galloping vibration when the cylinders are elastic. The interaction between boundary layer and cylinder also may generate galloping vibrations.

Keywords: *cylinders, forces, Strouhal numbers, flow structures, instabilities, interactions.*

NOMENCLATURE

a	Amplitude of vibration
C_D	Time-mean drag coefficient ($= F_D/(0.5\rho U_\infty^2 DL$)
C_{Df}	Fluctuating (root-mean-square) drag coefficient ($= F_{Drms}/(0.5\rho U_\infty^2 DL$)
C_L	Time-mean lift coefficient ($= F_L/(0.5\rho U_\infty^2 DL$)
C_{Lf}	Fluctuating (root-mean-square) lift coefficient ($= F_{Lrms}/(0.5\rho U_\infty^2 DL$)
C_{Li}	Instantaneous lift force
D	Diameter of cylinder
ζ	Damping ratio
ρ	Density of fluid
F_D	Drag force on cylinder
F_L	Lift force on cylinder
f_n	Natural frequency of a cylinder system
f_v	Vortex shedding frequency

L Length of load cell
m^* Mass ratio [(cylinder mass)/(fluid mass for the same volume of the cylinder)
Re Reynolds number ($= \rho U_\infty D/\mu$)
St Strouahal number ($= f_v D/U_\infty$)
T Gap spacing between the cylinders
U_∞ Free-stream velocity
U_r Reduced velocity ($= U_\infty / f_n D$)
V Cylinder velocity
VE Vortex excitation
y Displacement of cylinder
θ Angular position measured from front stagnation
μ Viscosity of fluid
α Stagger angle, the angle between the free-stream flow and the line connecting the centers of the cylinders

INTRODUCTION

Cylindrical structures in a group are frequently seen on land and in the ocean. Mutual flow interaction between the structures makes the wake very excited or tranquil depending on the spacing between the structures. The excited wake-enhancing forces in some cases cause a catastrophic failure of the structures. Slender structures in groups have many engineering applications, for example, chimney stacks, tube bundles in heat exchangers, high-rise buildings, harvesting wave and tide energy from ocean, overhead power-line bundles, bridge piers, stays, masts, chemical-reaction towers and offshore platforms. Naturally, it is important to understand the proximity effect on aerodynamics associated with multiple closely spaced cylindrical structures. While much is known of the flow physics around a single isolated cylinder, not much is known at that around a cylinder neighboured by another. There is no doubt that flow physics around two cylinders is much more complex and complicated than that around a single cylinder, because of interference between the cylinders, between the wakes, among four shear layers, etc. The study of the aerodynamics of two closely separated structures is thus of both fundamental and practical significance.

The flow behind two cylinders has been previously classified based on T/D and α. See figure 1 for the definitions of the symbols. A number of approaches have been used to classify the fluid behaviour of circular cylinders. Based on the interference effect between the two cylinders, Zdravkovich (1987) divided the whole region of possible arrangements of two cylinders into four: (i) the proximity interference region, where the flow around one cylinder affects the other; (ii) the wake interference region, the near-wake flow of the upstream cylinder is unaffected by the downstream one; however, the downstream one is significantly affected by the upstream cylinder; (iii) the proximity and wake interference region, where both proximity and wake interference are significant; (iv) the no-interference region, where the wake of one cylinder does not affect the other. Sumner et al. (2000) conducted flow visualisation and particle image velocimetry (PIV) measurements for T/D = 1.0 ~ 5.0, α = 0° ~ 90° and Reynolds number Re = 850 - 1900 ($Re = U_\infty D/\nu$, where U_∞ is the free-stream velocity and ν is the kinematic viscosity), and divided the T/D-α plane into three: (1) the single-body flow regime, T/D = 1.0 ~ 1.125 and α = 0° ~ 90°, where two cylinders act like an isolated body with a single vortex-shedding frequency, (2) the small incidence angle regime, T/D > 1.125 and α = 0° ~ 20°, where shear layer reattachment or the impingement of vortices onto the downstream cylinder takes places, (3) the large incidence angle regime, T/D > 1.125, α = 20° ~ 90°, where vortex pairing, splitting, enveloping and synchronising occur. Gu and Sun (1999) measured the time-averaged pressure on two cylinders (T/D = 0.1 ~2.5 and α = 0° ~ 90°), and observed three distinct pressure distributions, viz. Patterns I_B, II_B, III_B, on the downstream cylinder, which occurred over $\alpha = 0^\circ$ ~ 9.65°, 9.7° ~ 15°, and 16° ~ 90°, respectively, at T/D = 0.7. The downstream cylinder was completely and partially submerged in the wake of the other, respectively, in Patterns I_B and II_B but not in Pattern III_B. All these classifications are useful from the engineering design point of view, though they do not provide detailed information on forces and the flow structure around the cylinders.

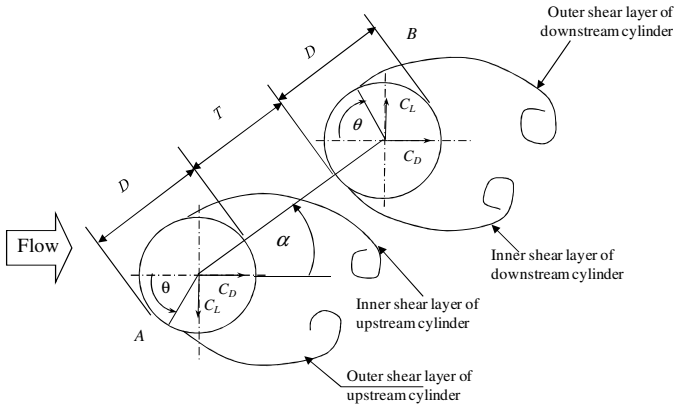

Figure 1 Notation of staggered configuration.

Time-mean drag and lift forces acting on two staggered cylinders have been examined in literature (e.g. Price 1976, Zdravkovich & Pridden 1977, Price & Paidoussis 1984), with most of the emphasis being on the downstream cylinder. Only a few studies have reported force measurements for the upstream cylinder (Gu & Sun 1999; Alam et al. 2003a, 2003b, 2005). Furthermore, fluctuating force measurements in the literature are very scant, though the fluctuating lift and drag forces acting on structures are a major cause of the fatigue failure of the structures and are used for predicting flow-induced responses. Most literature sources are connected to one of the three arrangements, tandem ($\alpha = 0^\circ$) or side-by-side ($\alpha = 90^\circ$) or staggered ($0^\circ < \alpha < 90^\circ$). Furthermore, flow classifications in the literature are based on either theoretical treatment (Zdravkovich 1987), or

experimental measurement of forces, *St* and pressure (e.g. Zdravkovich & Pridden 1977) or flow visualisation image (e.g. Peschard & Le Gal 1996). Determining the fluid dynamics from measured quantities is prone to misinterpretation, particularly when done without the benefit of accompanying flow visualisation. Articles with both measured quantities and flow visualisation are very few (e.g. Igarashi 1984). The present study measures all possible quantities including mean and fluctuating forces, *St* and pressure. Flow visualisation and surface oil-flow techniques are also employed to get insight into the physical flow around the cylinders and to get a better understanding of interactions.

Practically no structure is perfectly rigid, hence it is worthy to gain physical knowledge of flow-induced response of the structure. Bokaian & Geoola (1984a) investigated the case of two identical cylinders in tandem and staggered arrangements where the downstream one was fixed and the upstream one both-end-spring-mounted, allowing both ends to vibrate at the same amplitude (two-dimensional model) in the cross-flow direction only. They reported galloping vibration generated at spacing ratio of $T/D < 0.8$ (α =25°), $T/D \leq 0.75$ (α =0°) and vortex excitation (VE) at other T/D and α. Bokaian & Geoola (1984b) also investigated the other case where the upstream cylinder was fixed and the downstream one free to oscillate. Depending on T/D, the cylinder exhibited only galloping (T/D = 0.59, α =0°) or only VE (T/D > 1.5, α =0°) or a combined VE and galloping (T/D > 0.5, α =0°), or a separated VE and galloping ($1.0 \leq T/D \leq 1.5$). Note that the vibration always occurs at the natural frequency f_n of the cylinder. The VE corresponded to vibration occurring near the reduced velocity U_r (= $U_\infty/f_n/D$, U_∞ is the free-stream velocity) where the natural vortex shedding frequency f_v is close to f_n. On the other hand, the galloping vibrations persist for higher U_r corresponding to a higher f_v than f_n. In Bokaian & Geoola (1984a, b), the investigated ranges of T/D, α and mass-damping factor $m^*\zeta$ were 0.09~4, 0°~70° and 0.018~0.2, respectively, where m^* is the mass ratio and ζ is the damping ratio. Brika & Laneville (1997) response of the downstream cylinder with the upstream cylinder stationary or vibrating for T/D = 6 ~ 24, U_r = 4 ~ 21 (α = 0°). The system had a very low $m^*\zeta$ of 0.00007. When the upstream cylinder is stationary, the response of the downstream cylinder was no more hysteretic and it was strongly dependent on T/D; VE regime became wider and shifted to lower U_r with increasing T/d.

King & Johns (1976) investigated vibration characteristics of the downstream cylinder of two cylinders in tandem for spacing ratio T/D = 3.5 ~ 7. They observed the vibration of the downstream cylinder to be synchronized with that of the upstream cylinder. Also Ruscheweyh (1983) observed the downstream cylinder vibration in the wake of the upstream cylinder, and the vibration was termed as the wake-galloping. There are a few studies on flow-induced vibration of two cylinders arranged in staggered. Among them, Lam & To (2003) studied the vibration characteristics of the downstream cylinder having diameter half of the upstream cylinder. Tandem, side-by-side and staggered arrangements were considered. They observed both vortex-excited and galloping vibrations in staggered arrangement, only vortex-excited vibration in side-by-side, and none of them in tandem. Also, Brika & Laneville (1999) examined vibration characteristics of the downstream cylinder placed behind a fixed upstream cylinder with a large T/D = 13 and α = 5°, 10°, 15° and 20°. They observed only VE vibration, regardless of α. As mentioned above, the most studies are concerned with tandem arrangement and linked with vibration of the downstream cylinder when the upstream cylinder is fixed. As the wake of a vibrating cylinder depending on vibration amplitude is different from that of a stationary one (Williamson & Roshko 1988; Williamson & Govardhan 2004), it is expected that vibration response of the downstream cylinder would be different depending on whether the upstream cylinder is fixed or vibrating. Similarly, vibration response of the upstream cylinder may be affected by a feed back of the downstream cylinder vibration, at least for smaller T/D. Due to mutual interaction between two vibrating cylinders, more violent vibrations may be generated, compared with those when one of them is fixed.

Kim et al. (2008, 2009) and Alam & Kim (2009) conducted a systematic investigation on flow-induced response characteristics of two circular cylinders α = 0°, 5°, 10°, 15°, 25°, 45°, 60°, and 90°, T/D ranging from 0.1 to 3.2, At each position (α, T/D) of the cylinders, dependence of vibration-amplitude-to-diameter ratio a/D on reduced velocity U_r was examined. There were seven cylinder-response patterns, depending on whether vortex-excited and/or galloping vibrations of the cylinders are generated. Pattern I, either cylinder does not experience any excitation, i.e., no vibration is generated. Pattern II, the upstream cylinder does not vibrate but the downstream one experiences a galloping vibration. Pattern III, the upstream cylinder involves a galloping vibration only and the downstream one both VE and galloping. Pattern IV, both cylinders experience a VE; galloping vibration is however absent. Pattern V, the downstream cylinder only experiences VE. Pattern VI, VE of the downstream cylinder is generated in two regimes of U_r, while that of the upstream cylinder in one regime only. Pattern VII, both cylinders experience VE, but at two different regimes of U_r.

The objectives of this study were for two stationary rigid cylinders (i) to classify the flow regime globally based on forces, *St* and flow structures, (ii) to elucidate the flow structure for each regime, (iii) to find possible interaction mechanisms, and (iv) to find possible discontinuities and the respective instabilities responsible for them. Another objective of the study was to correlate interaction mechanisms and flow-induced response of the cylinders mounted elastically. The possible range of $\alpha = 0^\circ \sim 180^\circ$ were considered with T/D = 0.1 ~ 5.0. Flow-induced response results are mostly incorporated from literatures published by these authors and others.

EXPERIMENTAL DETAILS

Experiments were conducted at the fluid mechanics laboratory of Kitami Institute of Technology, Japan. Measurements were done in a low-speed, closed-circuit wind tunnel with a test section of 1.20 m in height, 0.30 m in width, and 2.2 m in length. Fluid forces, *St*, and cylinder-surface pressure measurements and surface oil-flow visualisation were conducted in this wind tunnel at a *Re* of 5.52×10^4 based on the diameter of a single cylinder. The turbulent intensity was 0.5%. More details of the tunnel are given in Alam *et al.* (2005). Figure 1 is a schematic diagram showing the arrangement of two cylinders, definition of symbols and coordinate systems. The stagger angle α is defined as the angle between the free-stream flow and the line connecting the centres of the two cylinders. *T* is the gap width between the cylinders, as opposed to centre-to-centre spacing adopted by other researchers. Fluid forces were measured over a small spanwise length of the cylinders, using load cells. The cylinder to be measured was built in with an active ('live') section of a spanwise 45 mm (0.92*D*) length and two dummy sections. This size was determined taking into account the cross-correlation length of fluctuating pressure in the spanwise direction of the cylinder. More details of the laodcell can found in Alam et al (2005). In this study, the repulsive (outward-directed) lift force is considered to be positive and the attractive (inward-directed) lift force is considered to be negative.

St was estimated from spectral analysis of the fluctuating pressures measured on side surfaces of the cylinders. The position of a point on the surface of a cylinder is defined by the azimuth angle θ, measured from the direction of free-stream flow. θ is considered $0^\circ \sim 180^\circ$ for the outer surfaces and $180^\circ \sim 360^\circ$) for the inner surfaces of the cylinders. Cylinder *A* is tentatively assumed to be fixed, and traversing of Cylinder *B* can be done with variation of the two parameters *T/D* and α. Experiments were performed for α = 0°, 10°, 25°, 45°, 60°, 75°, 90°, 105°, 120°, 135°, 155°, 170°, and 180°, for the spacing ratio of *T/D* = 0.1 ~ 5. Very fine-tuning of *T/D* was adopted with *T/D* = 0.1, 0.2, 0.3, 0.5, 0.6, 0.7, 0.8, 0.9, 1.1, 1.2, 1.5, 1.8, 2.1, 2.4, 2.7, 3.0, 3.5, 4.0, 4.5 and 5.0.

Flow visualisation was carried out in a water channel with a 250 × 350 mm working section and 1.5 m in length. A fine-mesh honeycomb was used to remove any large-scale irregularities. Two circular tubes with identical diameters of 20 mm were used. The Reynolds number in the water channel experiment was 350. This Reynolds number is beyond the transition range to turbulent in wake, as fully turbulent shedding conditions prevail for *Re* > 300 (Williamson 1996). The flow was visualised by using the hydrogen bubble technique, involving a platinum wire of 0.02 mm in diameter.

FLUID FORCES AND STROUHAL NUMBERS

Time-averaged drag coefficient (C_D), time-averaged lift coefficient, (C_L), fluctuating drag coefficient (C_{Df}) and fluctuating lift coefficient (C_{Lf}) are plotted in a *T/D*-α plane, and then the contour maps are drawn, as shown in figures 2 and 3. In the scale bars, the colour or the range marked by black '*' indicates the value of a single isolated cylinder. The result is described with reference to figure 1, in which Cylinder *A* is fixed, and traversing of Cylinder *B* is done with variation of the two parameters *T/D* and α, which suffice to determine the possible arrangement of the two cylinders. It may be noted that Cylinder *B* acts as the downstream and upstream cylinders for $|\alpha| < 90^\circ$ and $|\alpha| > 90^\circ$, respectively, i.e. the left and right sides of a contour map show the values of coefficient of the upstream and downstream cylinders, respectively. At the peripheries of the inner and outer circles, the values of *T/D* are 0.0 and 5.0, respectively. Note that the values of C_D, C_{Df}, C_L, C_{Lf} and *St* of a single cylinder are 1.12, 0.14, 0.00, 0.48 and 0.186, respectively. Repulsive and attractive C_L are considered as positive and negative, respectively.

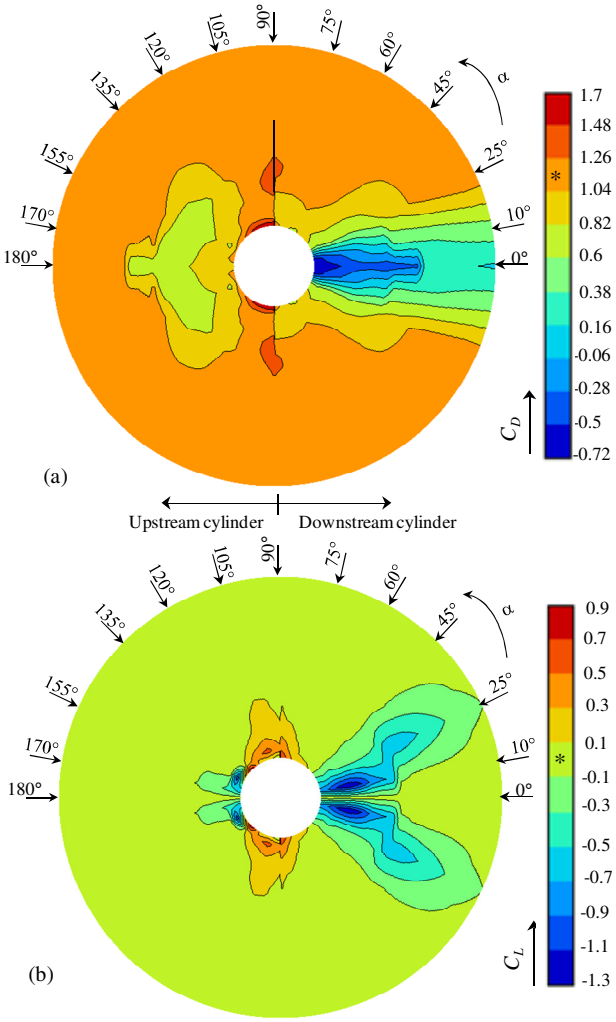

Figure 2 Contour maps of (a) time-mean drag coefficient C_D and (b) time-mean lift coefficient C_L. Points marked by '*' denote values of coefficients of an isolated cylinder.

The contour maps show that fluid force coefficients in the downstream region (right half) briskly change with changes in T/D and α; however, the upstream region (left half) retains single-cylinder values for $T/D > 3.0$ for any value of α. This signifies that the interference effect of the upstream cylinder on the downstream cylinder is much stronger but the opposite is rather weak.

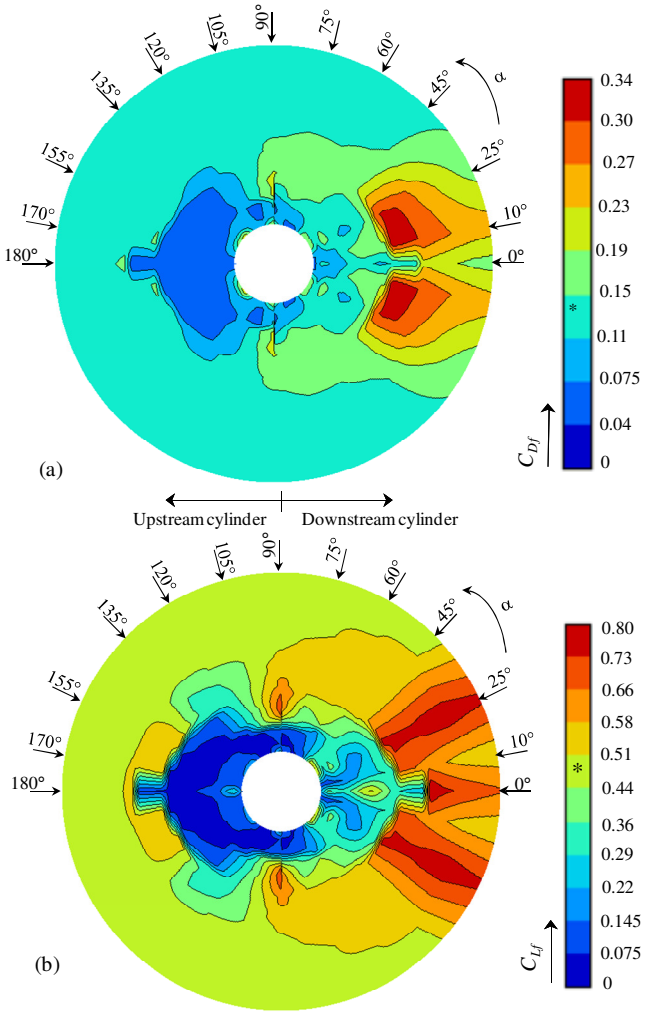

Figure 3 Contour maps of (a) fluctuating (r.m.s.) drag coefficient C_{Df} and (b) fluctuating (r.m.s.) lift coefficient C_{Lf}. Points marked by '*' denote values of coefficients of an isolated cylinder.

As seen in figure 2(a), the upstream cylinder experiences somewhat lower C_D at $|\alpha| > 120^\circ$, $T/D < 3.0$ than a single isolated cylinder. The downstream cylinder experiences highly negative C_D at $|\alpha| < 10^\circ$, $T/D < 3.0$, with a global minimum value of - 0.72 at $\alpha = 0^\circ$, $T/D = 0.1$. Maximum C_D of 1.26 ~ 1.48 and 1.48 ~ 1.7 acts on the cylinder at $\alpha \approx 90^\circ$, $T/D = 1.2 \sim 2.0$ and $\alpha = 90^\circ \sim 120^\circ$, $T/D < 0.2$, respectively. While enhanced coupled-vortex shedding is responsible for the higher C_D in the former region, there is perfectly single-body flow for later region. C_L = -1.03 and - 1.15 ~ - 1.25 are the minimum (most negative) values occurring at $|\alpha| = 155^\circ$, $T/D = 0.3$ and $\alpha = 10^\circ$, $T/D = 0.8 \sim 1.1$, respectively. C_L becomes maximum of 0.85 at $|\alpha| = 135^\circ$, $T/D = 0.1$.

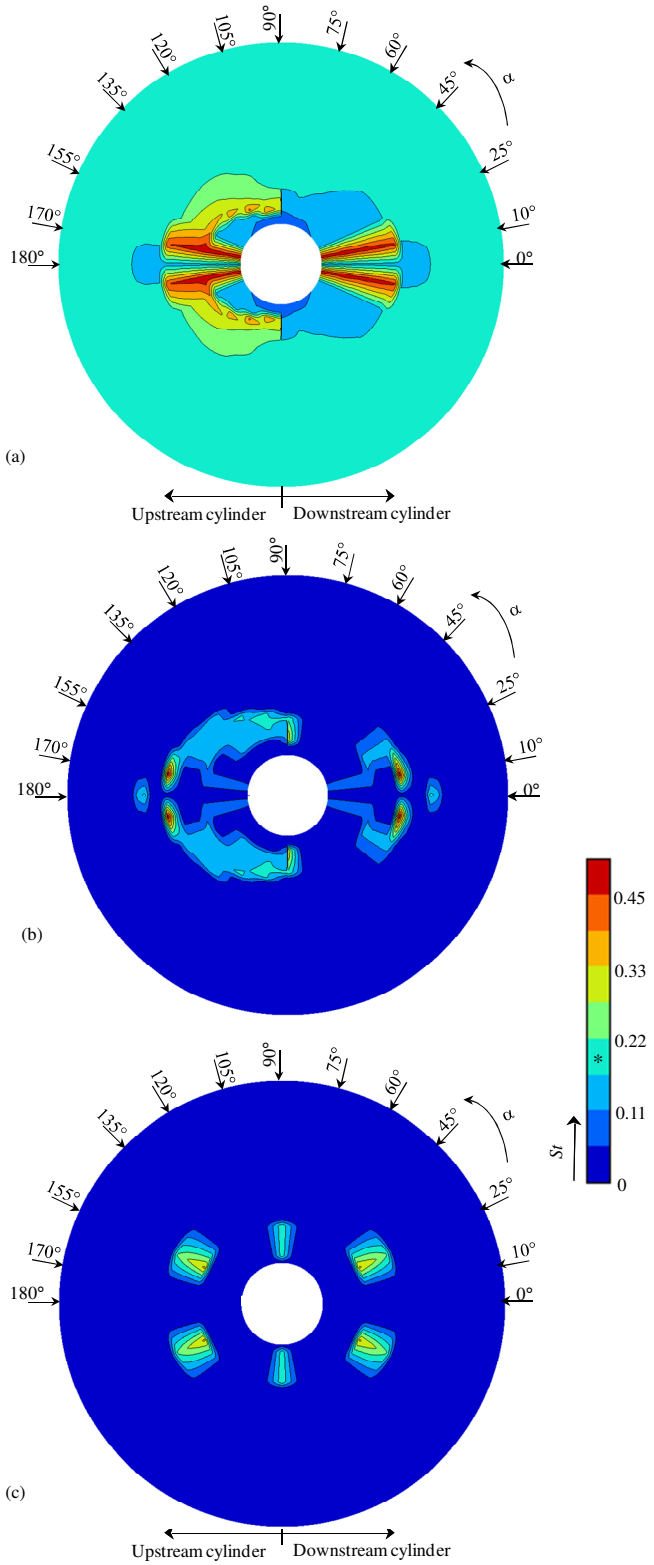

Figure 4 Contour maps of Strouhal number St. (a) primary mode, (b) secondary mode, (c) tertiary mode. Point marked by '*' denotes St value of an isolated cylinder.

Significantly higher C_{Lf} and C_{Df} act on the cylinder at $\alpha < 35^\circ$, $T/D > 2.5$ (figure 3). While the global maximum value of C_{Lf} is 0.8, 1.58 times the single-cylinder value, that of C_{Df} is 0.34, 2.35 times the single-cylinder value. On the other hand, C_{Lf} and C_{Df} are extremely small for $|\alpha| > 60^\circ$, $T/D <$

3.0. The observation suggests that the interference effect not only has a negative impact with increasing forces, but also a positive impact with reducing forces on the cylinder. Its impact, however, depends on α and T/D.

Figure 4 shows iso-contours of St in T/D - α plane. At bistable or tristable flows regions, there are more than one St corresponding to the individual flow structures. While figure 4(a) displays the primary dominant St, figures 4(b) and (c) display secondary and tertiary St. Therefore, the highlighted regimes in figures 4(b) and (c) imply the regimes of the bistable and tristable flows regarding St. The lowest St is 0.06 ~ 0.11 at $|\alpha| = 60^\circ \sim 120^\circ$, $T/D < 0.5$ (figure 4a) and the highest St is 0.45~0.5 at $|\alpha| = 10^\circ$, $T/D < 2.5$ (figure 4a). A scrupulous observation on the St map (figure 4) unveils that St has a strong relationship with C_D and/or C_L, but less with C_{Lf} or C_{Df}: St is inversely related with C_D and/or C_L. Where C_D or C_L is large in magnitude, St is lower and vice versa.

FORCE REGIMES AND FLOW STRUCTURES

In the previous section, brisk variations in C_D, C_L, C_{Df}, C_{Lf}, and St with change in T/D and α have been observed, implying that interference between the two cylinders, between the two wakes, and among four shear layers results in different fluid dynamics around, behind and between the cylinders depending on T/D and α. The interference gives rise to flow separation, recirculation, bubble formation, coupled and quasi-periodic vortices and instabilities of the gap flow, shear layers and wakes. As a matter of fact, 19 distinct flow regimes have now been identified as illustrated in figure 5, which is sketched based on rigorous observation of figures 2, 3 and 4. The features of each regime are described as follows:

①: ***No-interference regime***. C_D, C_L, C_{Df}, C_{Lf}, and St are almost the same as those of a single isolated cylinder. At this region, the cylinder is not interfered by the other.

②: ***Upstream-cylinder vortex-suppressed regime***. Reduced C_D, zero C_L, very low C_{Df} and C_{Lf}, and high St. The low magnitude of forces is attributed to the fact that for $|\alpha|$ = 170°-180°, the downstream cylinder acts as a stabiliser of the upstream-cylinder wake propelling the vortex formation (figure 6a$_1$), and for the rest $|\alpha|$ (=150° ~ 170°) formation of fully developed Karman vortex behind the upstream cylinder is retarded by the presence of the downstream cylinder (figure 6a$_2$). The high St is due to a retreat of vortex formation length (figure 6a$_1$). In general, forces (particularly C_D) and St are inversely correlated (Alam & Zhou 2007a, 2008).

③: ***Excited upstream-cylinder flow regime***. Somewhat increased C_{Df} and C_{Lf}; due to appearance of fully developed Karman wake and enhanced rolling of the upstream-cylinder shear layers. The downstream cylinder barring the shear layers thrusts them to roll strongly (figure 6b).

④: ***Highly deflected gap flow regime***. Attractive (negative) C_L, low C_{Lf} and low St. Highly deflected gap flow towards the upstream-cylinder wake causes attractive C_L (figure 6c), providing anticlockwise circulation around the cylinder. No Karman vortex shedding just behind the upstream cylinder results in the low C_{Lf}. The two cylinders behave like a single body, forming a single wake with alternating Karman vortex, hence corresponding to a low St. This regime includes a bistable flow regime marked by a shadow. Intermittent formation (figure 6c$_2$) and burst (figure 6c$_3$) of separation bubble on the gap-side surface of the upstream cylinder cause such a bistable flow being responsible for a large difference in C_L on the upstream cylinder. However, St values for both cases were the same, because the outer shears of the cylinders mainly govern the vortex shedding. Intermittent formation and burst were not possible to be observed in visualization because of the low Re (=350), but were observed in force and pressure measurements (Re = 5.52×10^4). See Alam et al. (2005) for the details of the bistable flow.

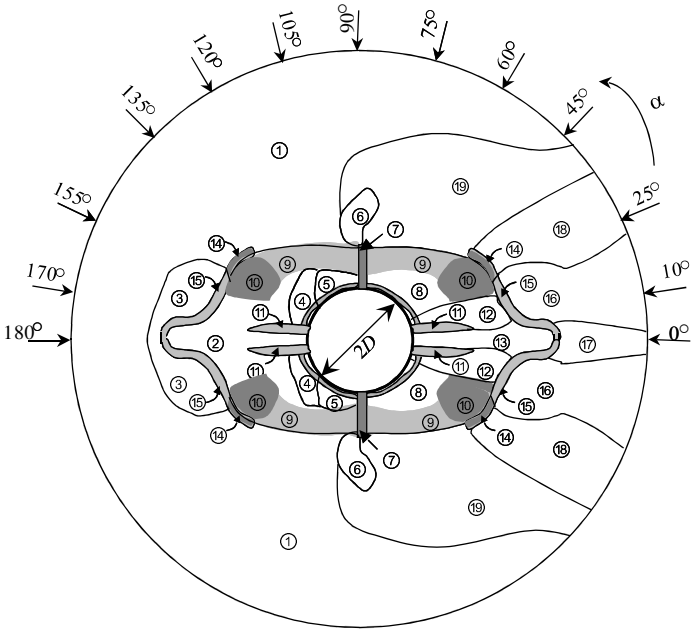

Figure 5 Sketch specifying various regions. The regions marked by shadows are multistable flow regions

⑤: ***Perfectly single-body regime***. Very high C_D, repulsive (positive) high C_L, low C_{Lf} and C_{Df} and low St. The two cylinders act as a single bluff body, resulting in a high C_D and low St (figure 6d). This regime also incorporates a bistable flow regime marked by a shadow. A turbulent reattachment and detachment of the inner-shear layer of the upstream cylinder initiate the bistable flow. Typical lift force signal showing the bistable nature of flow at T/D = 0.13 is presented in figure 7. Note that while only a stable reattached flow was observed at $T/D \leq 0.10$, only a detached flow at $T/D \geq 0.20$. The bistable flow is owing to intermittent turbulent reattachment and detachment of

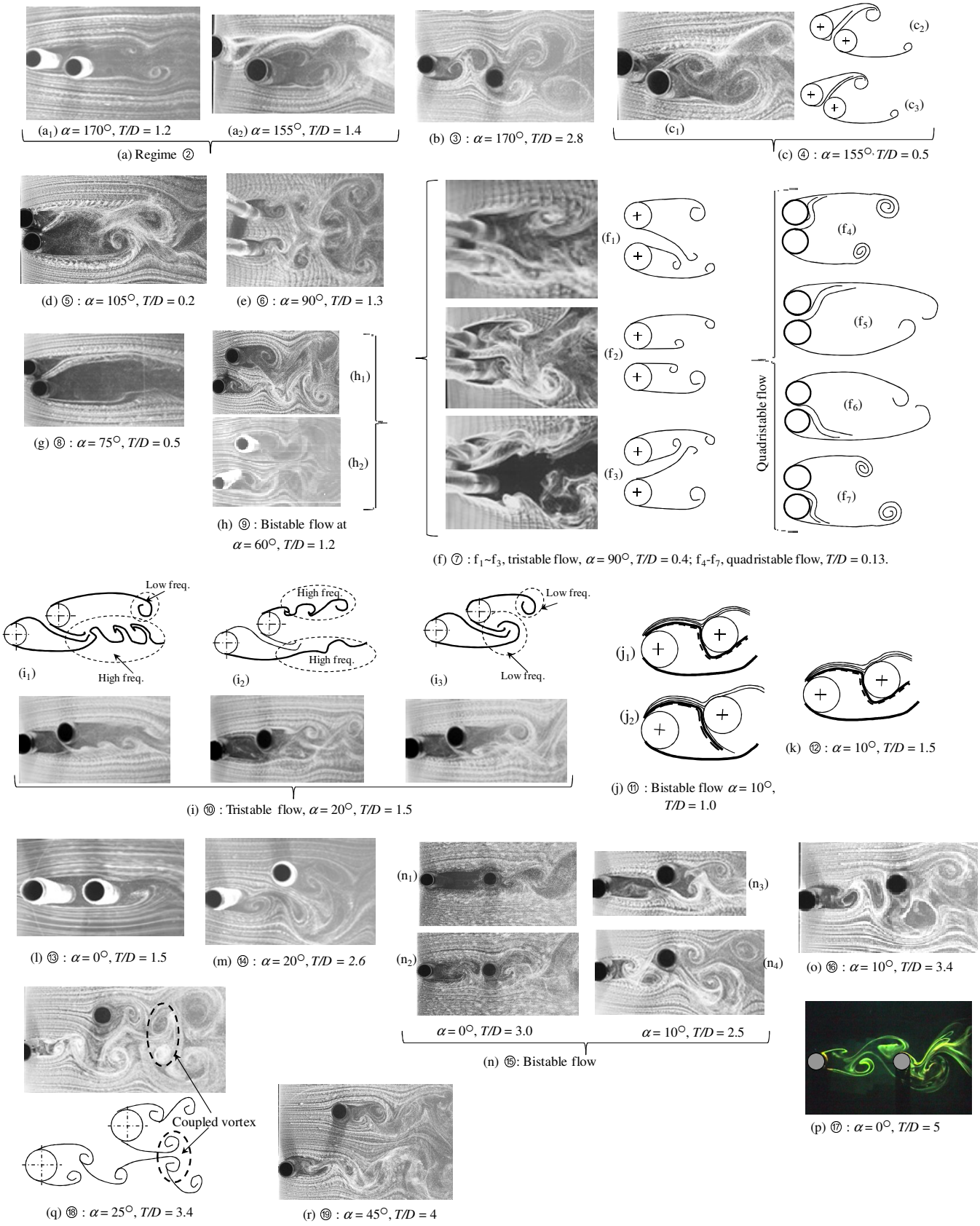

Figure 6 Representative flow structures at different regions.

the inner shear layer of the upstream cylinder.

⑥ : ***Antiphase vortex-shedding regime***. Very high C_D, repulsive C_L, high C_{Df} and C_{Lf}. Vortex shedding from one cylinder is constantly coupled with that from the other in an antiphase fashion, with their frequencies identical, which is referred to as antiphase vortex shedding. The antiphase shedding fortifying the Karman vortices is highly coherent, responsible for the high C_D, C_{Df} and C_{Lf}

(figure 6e). A predominance of antiphase shedding was also observed by Williamson (1985), Peschard & Gal (1996) and Meneghini et al. (2001). Also, for two square cylinders in side-by-side arrangement, Alam et al. (2010a) observed highly correlated anti-phased vortex shedding which resulted in a high C_D, C_{Df} and C_{Lf}.

⑦: ***Tristable and quadristable flip-flopping flow regimes***. Three modes of the flow, consider the upper cylinder, associated with wider wake, symmetric wake and narrow wake, are generated and switch from one to another (figure $6f_1$-f_3). The corresponding *St* observed are low (figure 4a, $\alpha = 90°$-), intermediate (figure 4c, $\alpha = 90°$), and high (figure 4b, $\alpha = 90°$-), respectively. The three *St* maps (figure 4a, b and c) indeed reflect the view that the side-by-side arrangement ($\alpha = 90°$) is the critical geometry between two staggered configurations of $\alpha = 90°$- and 90°+. For $\alpha = 90°$- (say $\alpha = 85°$), the gap flow is away from the upper cylinder (wide wake) corresponding to the lower *St* (figure 4a); for $\alpha = 90°$+ (say $\alpha = 95°$), the gap flow biases towards the upper cylinder (narrow wake) corresponding to the higher *St* (figure 4a). $\alpha = 90°$ should correspond to a symmetric wake (non-biased gap flow) with intermediate *St* (figure 4c). Hence, for $\alpha = 90°\pm$, the three flow modes appear intermittently, switching from one to another. Thus the tristable flow ensues from instability of the gap flow, appearing at $T/D = 0.2 \sim 1.2$. This regime includes a quadristable flow appearing at $T/D = 0.1 \sim 0.2$, caused by simultaneous instabilities of the gap flow and a separation bubble (figure $6f_4$-f_7). Typical lift force signal shown in figure 8 illustrates the details.

⑧: ***Single-body-like regime***. Reduced C_D, C_{Df} and C_{Lf} and a single low *St* in either wake. The two cylinders behave like a single body, giving a larger effective bluff width, generating weak vortex shedding from the two outer sides of the cylinders (figure 6g). Thus a single low *St* persists in the wake. The gap flow acting as a base bleed postpones the shear layers rolling, hence reducing C_D, C_{Df} and C_{Lf}.

⑨: ***Wake lock-in bistable flow regime***. Reduced C_D, C_{Df} and C_{Lf} , and two and one *St* values for the upstream- and downstream-cylinder wakes, respectively (figure 4a, b). Generally, the upstream-cylinder wake being narrow generates vortices at a higher frequency than the downstream cylinder (figure $6h_1$). Since the two wakes are in close proximity, the upstream-cylinder wake locks in to that of the downstream cylinder (figure $6h_2$), generating vortices at frequency of the downstream-cylinder wake, i.e. the two wakes are locked in. The lock-in occurs intermittently, with a flow switching from figure $6h_1$ to h_2 and vice versa. Therefore, the upstream cylinder generates vortices at two *St* (the low and high), while the downstream cylinder at one *St* (the low) (figures 4a, b).

⑩: ***Shear-layer-lock-in tristable flow regime***. Curtailed C_D, C_{Df} and C_{Lf} and two *St* values for the upstream and downstream cylinders. Three modes of flow with regard to vortex-shedding frequencies appear intermittently. They are: (i) the flow with a high *St* for the gap flow and the outer shear layer of the upstream cylinder and a low *St* for the outer shear layer of the downstream cylinder (figures 4a, $6i_1$), (ii) the flow with a high *St* for both cylinders (figures 4b, $6i_2$): lock-in of the downstream-cylinder shear layers to the upstream ones, and (iii) the flow with a low *St* for both cylinders: lock-in of the upstream-cylinder shear layers to the downstream ones (figures 4c, $6i_3$). See wavelet analysis results by Alam & Sakamoto (2005) for more view. Thus the tristable flow is caused by instabilities of the shear layers.

⑪: ***Bubble-burst bistable flow regime***. Highly negative C_L (-1.21). The bistable flow results from intermittent formation and burst of a separation bubble formed on the inner-side surface of the downstream cylinder (figure 6j). The mode, in which separation bubble persists, results in a highly negative C_L. This regime is characterized by a negative lift peak known as 'inner-lift peak regime' (Cooper 1973, Wardlaw & Cooper 1973, Price 1976, Zdravkovich & Pridden 1977). The researchers observed rapid changes in the mean lift force for small adjustments to the geometry, which was attributed to the high-speed flow deflected through the gap between the cylinders. The explanation was not so specific, hence later Alam *et al.* (2005) with pressure measurement and surface oil-flow results showed that the lift peak is mainly due to a separation bubble forming on the inner side of the cylinder and the rapid change in mean lift is connected to the formation and burst of the separation bubble. In fact the global minimum C_L (-1.21) occurs at this regime. Since only one wake is formed behind the cylinders, *St* of the two cylinders in a mode is the same, a high ($St \approx 0.47$) and low ($St \approx 0.09$) for the modes with and without bubbles, respectively (figures 4a, b).

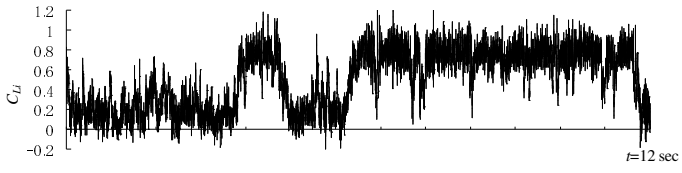

Figure 7 Lift force signal of the upstream cylinder for $\alpha = 105°$, $T/D = 0.13$, indicating bistable nature of flow. (Alam *et al.* 2005).

⑫: ***Separation-bubble flow regime***. Attractive C_L, and high *St*, resulting from a separation bubble formed (figure 6k). The flow structure is similar to the separation-bubble mode (figure $6j_1$) appearing in regime ⑪. Therefore, *St* is very high and C_L is still negative.

⑬: ***Fully submerged flow regime***. Zero C_L and highly negative C_D. The downstream cylinder is fully submerged in the wake of the upstream cylinder (figure 6l). The most negative C_D of -0.72 happens in this regime.

⑭ : ***Vortex-triggered tristable flow regime***. The upstream-cylinder wake is generally narrow and the downstream one is wide, corresponding to a high and low *St*, respectively. The convective vortices from the upstream cylinder sometimes trigger the vortex shedding from the downstream cylinder, forcing the downstream cylinder to shed vortices at the higher *St*. The three modes of flow are: (i) the flow with a higher and lower *St* for the upstream and downstream cylinders, respectively, (ii) the flow with the higher *St* for both cylinders, and (iii) the flow with synchronised *St* approximately equal to that of a single cylinder. The first and second modes with a thicker flow through the gap resemble those (figure 6i_1, i_2) in regime ⑩. The third mode is given in figure 6(m). This regime is in fact a transition regime in which fully developed flow behind the upstream cylinder starts to form. This regime is in fact a transition regime in which fully developed flow behind the upstream cylinder starts to form. Therefore, jump in fluctuating forces (figure 3a, b) and *St* (figure 4a, b) occurs.

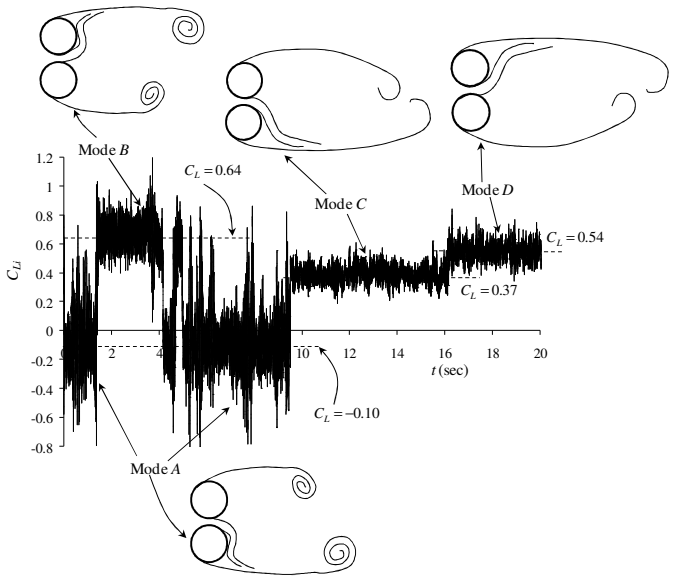

Figure 8 Time history of instantaneous lift force on the lower cylinder at $T/D = 0.13$ and flow sketches corresponding to the different modes of lift force (Alam & Zhou 2007b).

⑮: ***Shear-layer-reattachment bistable flow regime***. Two flow patterns appear alternately. For $\alpha = 0^\circ$, i.e. in-tandem arrangement, the shear layers separating from the upstream cylinder reattach steadily onto the downstream cylinder (figure 6n_1) or strongly roll up behind the upstream cylinder (figure 6n_2), and for $0^\circ < \alpha < 25^\circ$, only the inner-shear layer of the upstream cylinder reattaches onto the front surface of the downstream cylinder (figure 6n_3) or strongly rolls up before it (figure 6n_4). While the reattachment mode corresponds to a smaller fluctuating force (figure 3a, b) and high *St* (figure 4a), the roll-up mode corresponds to a larger fluctuating force (figure 3a, b) and *St* of approximately equal to that of a single isolated cylinder.

⑯: ***Vortex-triggered synchronised shedding regime***. Very high C_{Df}. The inner shear-layer of the upstream cylinder rolls just before the front surface of the downstream cylinder (figure 6o), causing a higher fluctuation of pressure on the front surface, hence a higher C_{Df} on the downstream cylinder. Though the downstream cylinder confronts a highly turbulent non-uniform approaching flow, its vortex-shedding frequency is the same as that of the upstream cylinder confronting a smooth uniform approaching flow. This happens due to the fact that the convective alternating vortices from the upstream cylinder trigger the vortex shedding of the downstream cylinder.

⑰: ***Co-shedding flow regime***. Very high C_{Lf}. It is engendered by an alternating buffeting of the upstream-cylinder vortices convective along the side surfaces of the downstream cylinder (figure 6p).

⑱: ***Synchronised coupled-vortex regime***. Extremely high C_{Lf} and attractive C_L. The inner-shear layer of the downstream cylinder sheds vortices in synchronisation with the convective inner vortices from the upstream cylinder, generating a coupled vortex, resulting in a higher fluctuating pressure on the inner-side surface of the downstream cylinder, hence the cylinder experiences a higher C_{Lf} (figure 6q).

⑲: ***Small interference regime***. Somewhat high C_{Df} and C_{Lf}; the downstream cylinder is outside the wake of the upstream cylinder; hence interference effect is trivial (figure 6r).

PHYSICAL INTERACTIONS

A single cylinder in cross-flow in general generates boundary layers, shear layers, alternating vortices and wake. When two cylinders are in close proximity, boundary layers, shear layer, vortex and wake are therefore four physical interacting parameters. A scrupulous observation of flow structures in figure 6 and the flow structure details reveals the following six types of interactions. They are interaction between (i) boundary-layer and cylinder, (ii) shear-layer/wake and cylinder, (iii) shear layer and shear layer, (iv) vortex and cylinder, (v) vortex and shear layer, and (vi) vortex and vortex. Their regimes are given in figure 9. Naturally, their boundaries include more than one flow type described in the earlier section. The details of the interactions are given as follows.

Boundary layer and cylinder interaction: this interaction occurs when *T/D* is small, $T/D < 0.3$ - 0.6 depending on α. Interacting with the other cylinder, boundary layer of a cylinder may form separation bubbles, delay to separate, reattach, etc. See figure 6c, d, g. The interaction therefore intensifies C_D and C_L but weakens C_{Df} and C_{Lf}. The two cylinders being very close behave like a combined cylinder.

Shear-layer/wake and cylinder interaction: this happens

when shear layer(s) from one cylinder interacts on the other cylinder surface by reattaching, impinging, forming separation bubble, etc. (figure 6j, k, l, n_1, n_3). Naturally, one of the cylinders is completely (figure 6l, n_1) or partially (figure 6j, k, n_3) submerged in the wake of the other, hence it can also be termed as wake and cylinder interaction. The shear layer interacted by the cylinder loses its strength to shed alternating Karman vortex, hence forces wane significantly. Being completely submerged in the wake of the other, the cylinder acting as a stabiliser suppresses the flow unsteadiness between the cylinders. The interaction occurs when two cylinders are nearly in-line, $|\alpha| \approx 0^\circ \sim 20^\circ$, $0.3 < T/D < 2.3$-3.

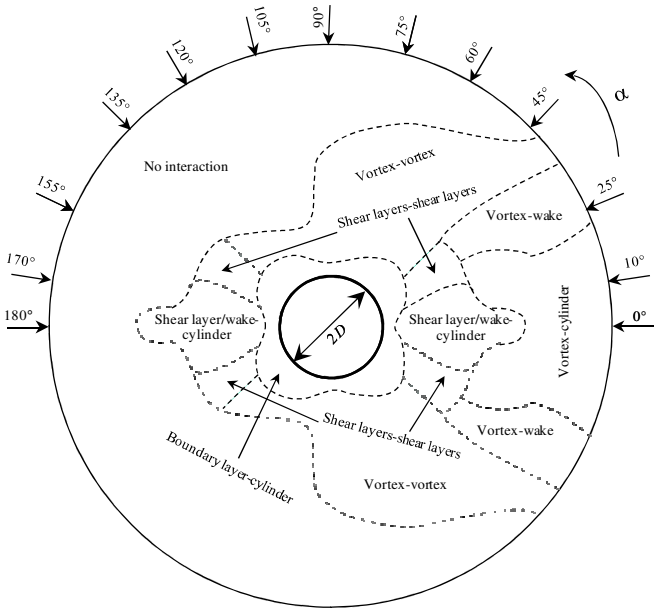

Figure 9 Possible interactions and their regimes in T/D-α plane.

Shear layer and shear layer interaction: here the shear layer(s) of a cylinder directly interacts with that of the other. The interaction causes intermittent interlock-in of the shear layers, hence generates vortices at more than one frequency (figure 6i), and reduces forces on the cylinders. Since α of this interaction is higher than that of shear layer/wake and cylinder interaction regime, generation of two shear layers through the gap is possible. The two shear layers interact with themselves and the outer-shear layers (figure 6i).

Vortex and cylinder interaction: when T/D is greater than the critical spacing of two nearly in-line cylinders, the shear layers of the upstream cylinder cannot reach the downstream cylinder, hence roll between the cylinders, forming alternate vortices. Thus the alternate vortices from the upstream cylinder strike on the downstream cylinder and embrace the side surface during passing on the cylinder (figure 6o, p). This interaction is generally very strong, intensifying C_{Df} significantly. Gursul and Rockwell (1990) investigated the interaction of oncoming two rows of vortices on an elliptical leading edge and observed very high fluctuating pressure on the surface where vortices reached.

Vortex and shear-layer interaction: for a larger α, the downstream cylinder becomes offset from the inner row of vortices from the upstream cylinder, hence the vortices cannot interact with the downstream cylinder, but can interact with the inner-shear layer. Interacting with the shear layer while it is growing, the vortices force the shear layer to form a synchronised coupled vortex (figure 6q). This interaction renders a very high C_{Lf}, as alternate interaction between vortex and shear layer intervenes.

Vortex and vortex interaction: for a further increase in α, the transverse distance between the cylinders becomes large, hence each cylinder forms a separate wake immediately behind them. The vortices on the two inner rows interact with each other and combine the two wakes into a wider one (figure 6e, f, r), which results in a slightly higher C_D, C_{Df} and C_{Lf}.

The above discussion on possible interactions and on their effects on forces bears physical insight into force and/or flow control mechanisms. As such, vortex and cylinder or vortex and shear layer interactions intensify forces, while shear-layer/wake and cylinder interaction reduces forces and the unsteadiness of the flow. In the literatures, aerodynamics and hydrodynamics means for reducing fluid forces are classified into four categories (Zdravkovich 1981; Alam et al. 2006).

(a) The control of shear layer by surface protrusion (tripping wire, fin, helical strakes, helical wires, studs, etc.), e.g. Alam et al. (2010b), or by placing a small cylinder in the shear layer, e.g. Alam et al. (2003c)

(b) The control of the entrainment layers by shrouds (perforated gauze, axial rods, etc.), which supply irrotational fluid to the entrainment layers, e.g. Knell (1969).

(c) The instability control of wakes by near-wake stabilisers (splitter plate, guiding plates, etc.), which reduces the interaction of two opposite shear layers, e.g. Bearman (1965).

(d) Approaching flow control by placing a small rod in front of the model, e.g. Sakamoto et al. (1997). Forces reduce when the shear layers from the rod attach on the cylinder.

As seen, categories (a), (c) and (d) belong to the interaction between boundary layer and cylinder or shear layer/wake and cylinder where C_{Df} and C_{Lf} are reduced most. Therefore, the interaction mechanism is the key factor to reduce or enhance forces or flow unsteadiness.

FLOW-INDUCED FREE VIBRATION

The all of the above results are for two fixed cylinders, elucidating physics of flow, interaction mechanisms, instabilities, interference, etc. How the interactions affect flow-induced instability of the cylinders, compared to a single isolated (non-interfering) cylinder, is of great interest to the researchers in science and engineering.

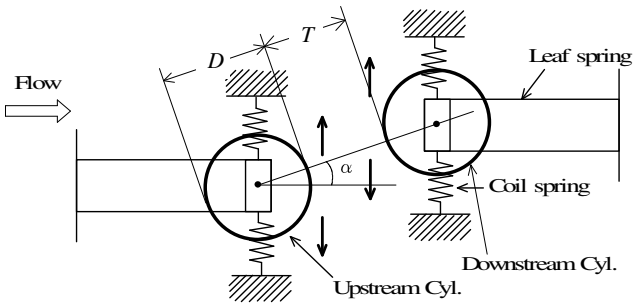

Figure 10 Free-vibration set up in wind tunnel

This section includes an overview of flow-induced vibration results for two elastically mounted cylinders (figure 10). The detailed results of cylinder responses at different interaction regimes are presented in figure 11. While the vertical axis of the response curves represents the vibration amplitude a normalized by D, the horizontal axis is U_r. The dimension in the vertical axis is not rendered because the vibration amplitude is generally dependent on $m^*\zeta$ and different literatures adopted different values of $m^*\zeta$. A lower $m^*\zeta$ corresponds to higher vibration amplitude and vice versa, keeping the trend almost the same. The response curve were mostly taken from Kim et al. (2008, 2009) and Alam & Kim (2010). The dashed line in the response graphs sands for single isolated cylinder response, insinuating VE at $U_r \approx 5.4$ ($\approx 1/St = 1/0.186$).

In the boundary layer and cylinder interaction regime, while both cylinders experience divergent galloping vibration for $U_r > 10$ at $0 < \alpha < 25°$ (figure 11a, d), they experience VE between $U_r = 7$ to 10 for $25° < \alpha < 155°$ (figure 11b, c). For the latter case, the downstream cylinder vibration amplitude is larger than the upstream one. Divergent violent vibrations of both cylinders are generated in the regime of shear-layer/wake and cylinder interaction (figure 11e, f, n, o). VE and galloping are combined at smaller T/D (figure 11e, o) and separated for larger T/D (figure 11f). High amplitude VE is afoot in the

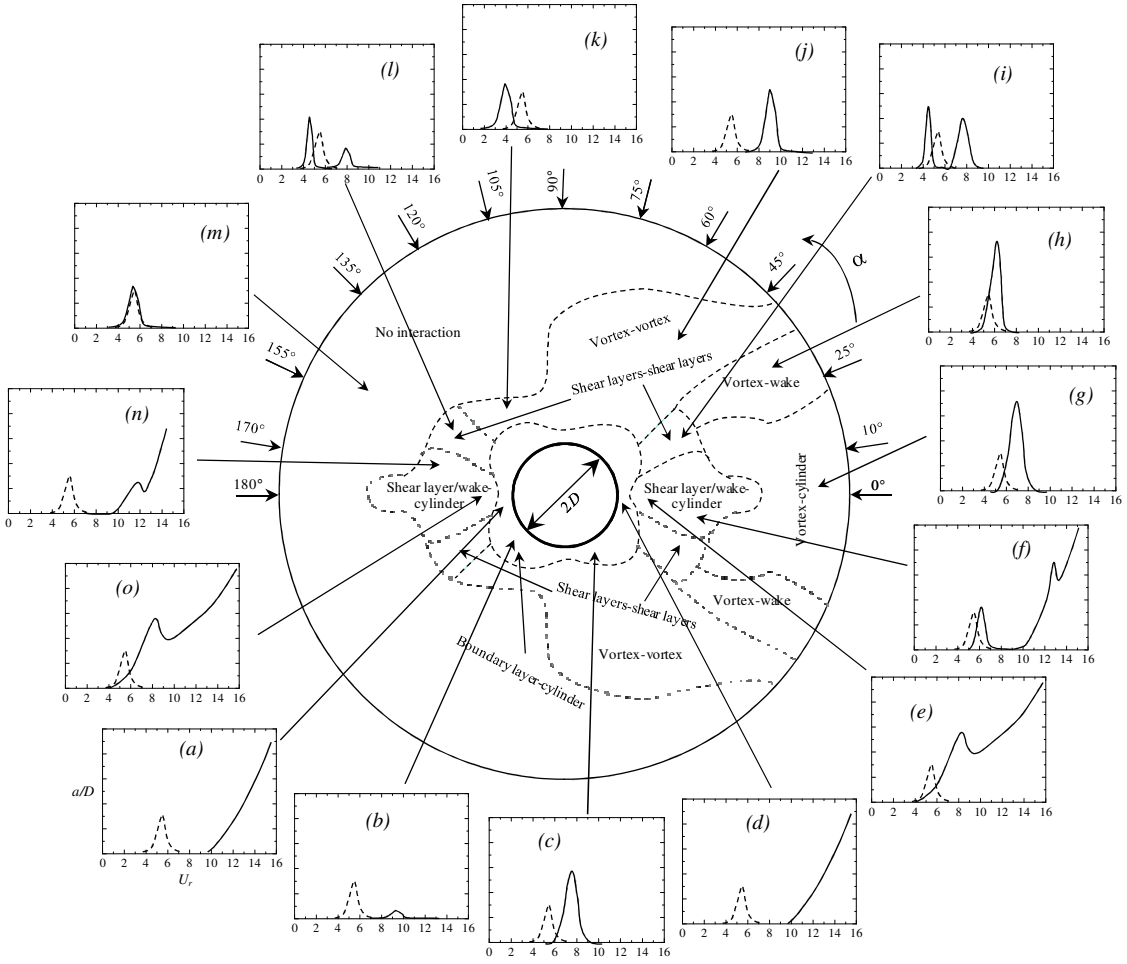

Figure 11 Flow-induced vibration response at different interaction regimes. Dashed line represents a single isolated cylinder response. The vertical and horizontal axes of the response graphs are the vibration amplitude ratio a/D and reduced velocity U_r (= $U_\infty/f_n/D$). The response curves are based on the results in Bokaian and Geoola (1984a, b), Kim et al. (2008, 2009), Borazjani and Sotiropoulos (2009) and Alam and Kim (2009).

regimes of vortex and cylinder interaction (figure 11g) and vortex and wake interaction (figure 11h), where fluctuating forces on stationary cylinders are high (figure 3). In the shear layer and shear layer interaction regime, VE occurs at two regimes of U_r (figure 11i, *l*). It has been shown that in this regime both cylinders shed vortices at two frequencies (figure 6i), hence corresponds to two VE. In the vortex and vortex interaction regime, VE intervene at a high U_r for the downstream cylinder (figure 11j) and at a low U_r for the upstream cylinder (figure 11k). This is due to fact that the downstream and upstream cylinders generally shed vortices at a low and high frequencies, respectively. The no interaction regime corresponds to VE at the same U_r as that of a single cylinder (figure 11m).

It is worthy to mention that a larger C_{Lf} (figure 3b) corresponds to larger amplitude VE (figure 11c, g, h). The most striking feature is that divergent galloping vibration is generated at shear layer/wake and cylinder interaction (figure

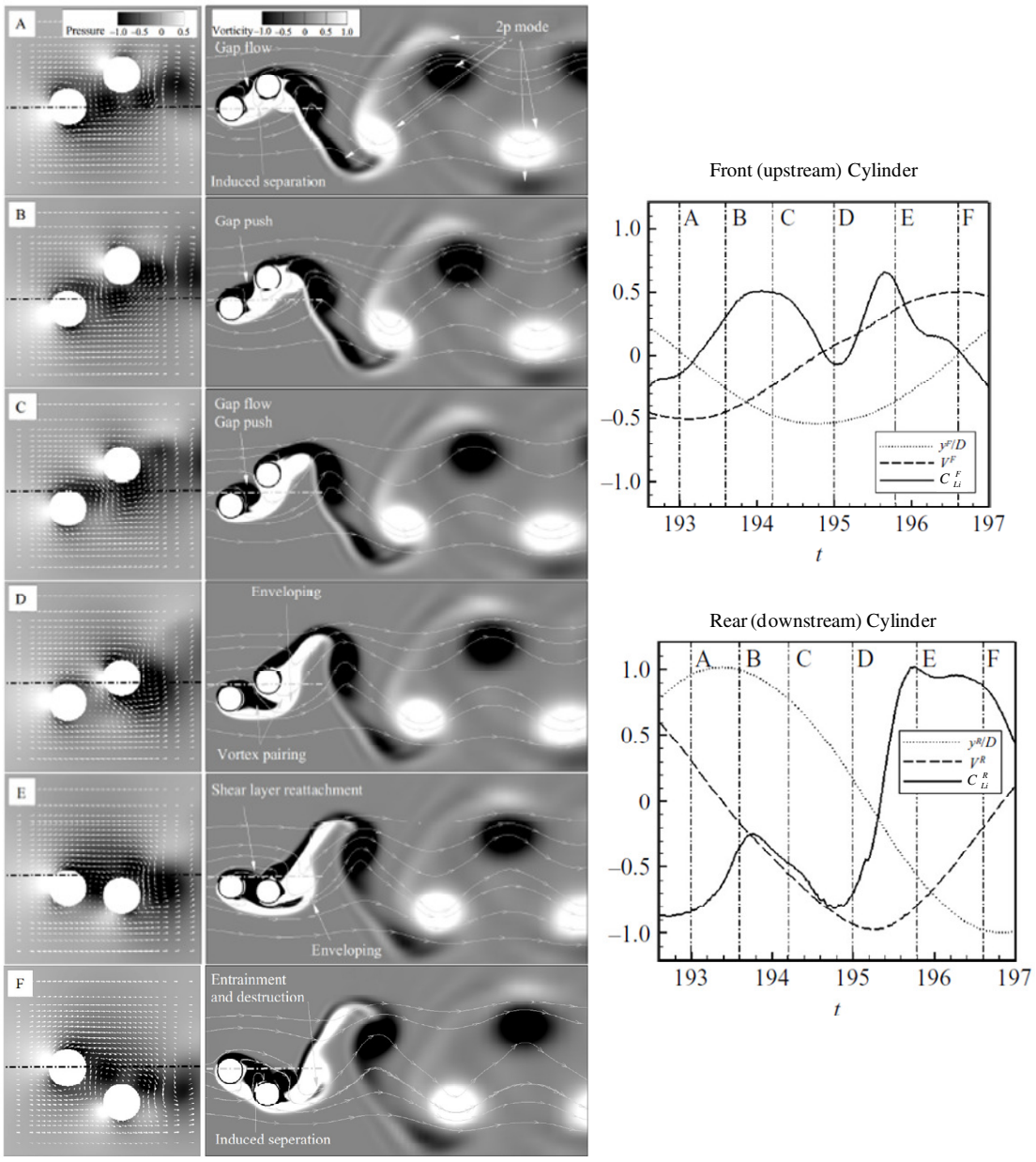

Figure 12 Velocity vectors with pressure contours (first column) and streamlines with vorticity contours (second column) for two cylinders corresponding to response in Figure 11(*a*) and 11(*l*) *at* U_r = 11. The horizontal dash-dotted lines in A–F indicate the initial rest positions of the cylinders. The time instants (A, B, C, . . .) are specified by the dash-dotted lines on the accompanying time history for the visualized portion of the cycle at the third column of the figure. The superscripts F and R refer to the front and the rear cylinders, respectively; *y/D* is the position of the cylinder; *V* is the velocity of the cylinder; C_{Li} is the instantaneous lift coefficient. Borazjani and Sotiropoulos (2009).

11e, f, n, o) and boundary layer and cylinder interaction (figure 11a, d) regimes where there is a large variation in C_L in the cross-flow direction (figure 2b). It is an acknowledged fact from galloping theories that galloping is not generated on axis-symmetric body, e.g. a circular cylinder. Therefore a question arises, why do two circular cylinders at close proximity experience galloping? In the regimes of boundary layer and cylinder interaction and shear layer/wake and cylinder interaction, the two cylinders are connected by boundary layer or shear layer, the combined shape of the two cylinders is not further axis symmetric, hence the two cylinders may prone to generate galloping vibrations. Furthermore, due to having non-uniform velocity between the cylinders, the downstream cylinder again is not axis symmetric with respect to local approaching flow. That is, the galloping generation for two circular cylinders at close proximity is not violating the galloping theories. In order to get insight into the flow physics during galloping vibration, figure 12 are shown in a half cycle during cylinder vibrations, displaying instantaneous velocity and pressure fields (first column), vorticity and streamlines (second column) and time histories of instantaneous lift C_{Li} and cylinder motion (third column).

Comparing motion histories of two cylinders (right column), it is evident the upstream (front) cylinder oscillation leads the downstream cylinder by 90° phage angle. figure 12(A) corresponds to the position where the rear cylinder is close to its top maximum position and the front cylinder is almost at the initial position. The downstream cylinder therefore incurs a stagnation pressure at its upper front and negative pressure on the lower side. The resulting pressure distribution on the rear cylinder is such that C_{Li} is negative (restoring) and thus out of phase with the positive displacement of the cylinder. The vorticity field also testifies that net circulation around the cylinder would be anticlockwise corresponding to a negative lift. Since between A and B, the average velocity of the front cylinder is higher than that of the rear cylinder of which velocity magnitude is very small, the lateral separation between the cylinder increases; therefore the rear cylinder stagnation pressure point shifts from upper front to front and the low pressure region recedes to the rear. Stagnation pressure point on the front cylinder on the lower front as it moves downward. C_{Li} for front cylinder is therefore positive and increases. Its magnitude for the rear cylinder decreases.

Between B and C, average velocity is smaller for the front cylinder than the rear one, thus lateral spacing decreases and the rear cylinder pushes the upper shear layer of the front cylinder into the gap region underneath the rear cylinder (figure 12C). By this interaction the low-pressure core from the front cylinder vortex shedding is advected further downstream and merged with the low-pressure pocket from the rear cylinder shedding, right underneath the rear cylinder, increasing the lift force on that cylinder. Also the low-pressure pocket on top of the front cylinder from the vortex shedding has become stronger by the gap push and the accelerated flow in the gap region. The direction of the lift force on both cylinders is therefore restoring.

The lateral spacing decreases further in figure 12(D), and the front cylinder reaches its minimum. Hence C_{Li} is almost zero on the front cylinder being approached by free stream. The 'vortex pairing' process causes the 'enveloping' of the negative vorticity from the displaced upper shear layer of the front cylinder by positive vorticity of the lower shear layers of both cylinders. The ensuing very complex vortex-to-vortex interactions lead to the rapid growth of the low-pressure region, which is now at the rear of the descending rear cylinder. This increases further the lift force that accelerates the rear cylinder, which has almost reached the initial position (y = 0) while travelling downward.

In E the ascending front cylinder now passes the descending rear cylinder. The gap flow has seized to exist, as the gap region is now occupied by a cell of recirculating, low-velocity flow. A pocket of high (stagnation) pressure has started forming at the lower front of the rear cylinder, as the cylinder is now outside of the wake of the front cylinder and is again exposed to the free stream velocity. The upper half of the gap region is in fact now occupied by a large pocket of low pressure, which results in a force that tends to accelerate the ascending front cylinder and retard the descending rear cylinder, eventually causing the rear cylinder to stop and reverse its direction of motion.

The time instant F marks the end of the first half of the cycle and is essentially the mirror image of the time instant A. A notable feature in the near wake of the second cylinder is the complete destruction of the negative vorticity that was previously enveloped by the positive shear layers.

The above discussion implies that a strong interaction between the front cylinder shear layer and the rear cylinder is responsible for the galloping vibration.

CONCLUSIONS

The investigation leads to the following conclusions.

C_D, C_L, C_{Df} , C_{Lf} and St of the cylinders are strong functions of α and T/D, connected to 19 distinct flow patterns, including one quadristable flow, three kinds of tristable flows and four kinds of bistable flows. The quadristable or tristable or bistable flow engenders strong jumps in C_D, C_L, C_{Df} , C_{Lf} and St of the cylinders. **Quadristable flow**: it is afoot in side-by-side arrangement at small T/D (= 0.1 ~ 0.2), resulting from simultaneous instabilities of the gap flow and separation bubble. **Tristable flow**: the three kinds of triastable flows appearing at different regimes have different characteristics. The 1st kind of tristable flow happening at regime ⑦ is due to instability of the gap flow forming a narrow wake, wide wake and symmetric wake. The 2nd kind appearing at regime ⑩ is caused by lock-in instability of the shear layers, with frequency lock-in of a shear layer to the others. The 3rd kind

occurring at regime ⑭ results from vortex-triggered synchronization. **Bistable flow:** the 1st kind of the bistable flow appearing at regime ⑮ is the instability of cylinder shear layers tending to attach/detach to/from the other cylinder. The second kind of bistable flow results from instability of a laminar separation bubble forming and burst on the cylinder surface, regimes ④ and ⑪. The third kind of bistable flow generated from instability of a shear layer susceptible to turbulent reattachment and detachment on the rear surface of the same cylinder, regime ⑤. The fourth kind of bistable flow results from instability of the two wakes in which the upstream cylinder wake intermittently locks-in to the downstream one with regard to vortex-shedding frequency, regime ⑨.

Six different interacting mechanisms between the cylinders were observed: boundary layer and cylinder interaction, shear layer/wake and cylinder interaction, shear layer and shear layer interaction, vortex and cylinder interaction, vortex and shear layer interaction, and vortex and vortex interaction. Each of them had different influences on the induced forces and *St*. There exist two island-like regimes (regimes ⑯: $\alpha = 10^\circ \sim 25^\circ$, $T/D = 2.2 \sim 4.0$; regimes⑱: $\alpha = 18^\circ \sim 32^\circ$, $T/D = 2.1 \sim 5$) where the values of C_{Df} and C_{Lf} are extensively high, about 2.35 and 1.58 times the single-cylinder values. The high values of C_{Df} and C_{Lf} are ascribed to vortex and cylinder and vortex and shear layer interactions, respectively. Both shear layer/wake and cylinder, and boundary layer and cylinder interactions weaken C_{Df}, C_{Lf} and flow unsteadiness. While the former interaction stabilises the wake or shear layers, the latter one forms a separation bubble, delays boundary layer separation, or causes reattachment. The separation bubble formation results in maximum repulsive C_L of +0.86 at $|\alpha| = 135^\circ$, $T/D = 0.1 \sim 0.2$. Maximum C_D of 1.75 acts on the cylinders in the regime of $|\alpha| = 90^\circ$, $T/D = 2.2 \sim 2.6$ (regime ⑥) caused by a strong vortex and vortex interaction, which is about 1.56 times the single-cylinder value.

Though a single non-interfering circular cylinder does not experience galloping, two circular cylinders incur violent galloping vibration due to shear layer/wake and cylinder interaction and boundary layer and cylinder interaction. In the case of VE, a stronger C_{Lf} corresponds to larger vibration amplitude.

ACKNOWLEDGENT

M.M. Alam wishes to acknowledge support given to him by the UP Research Development Programme through Grant No. A0T366 and by Monbukagakusho, Japan.

REFERENCES

Alam, M. M. & Kim, S. 2009 Free vibration of two identical circular cylinders in staggered arrangement. *Fluid Dynamic Research* 41, 035507, 17pp.

Alam, M. M., Sakamoto H. & Zhou, Y. 2006 Effect of a T-shaped plate on reduction in fluid forces acting on two tandem circular cylinders in a cross-flow. *J. Wind Engng Indust. Aerodyn.* 94, 525-551.

Alam, M. M., Sakamoto, H. & Moriya, M. 2003c Reduction of fluid forces acting on a single circular cylinder and two circular cylinders by using tripping rods. *J. Fluids Struct*. 18(3-4), 347-366.

Alam, M.M. & Sakamoto, H. 2005 Investigation of Strouhal frequencies of two staggered bluff bodies and detection of multistable flow by wavelets. *J. Fluids Struct*. 20(3), 425-449.

Alam, M.M. & Zhou, Y. 2007a The turbulent wake of an inclined cylinder with water running. *J. Fluid Mech.* 589, 261-303.

Alam, M.M. & Zhou, Y. 2008 Alternative drag coefficient in the wake of an isolated bluff body. *Phy. Review E* 78, No. 3, 036320-9.

Alam, M.M. and Zhou, Y., 2007b. Flow around two side-by-side closely spaced circular cylinders. *J. Fluids Struct*. 23, No. 5, 799-805.

Alam, M.M., Moriya, M. & Sakamoto, H. 2003a Aerodynamic characteristics of two side-by-side circular cylinders and application of wavelet analysis on the switching phenomenon. *J. Fluids Struct*. 18, 325-346.

Alam, M.M., Moriya, M., Takai, K. & Sakamoto, H. 2003b Fluctuating fluid forces acting on two circular cylinders in a tandem arrangement at a subcritical Reynolds number. *J. Wind Engng Indust. Aerodyn.* 91, 139–154.

Alam, M.M., Sakamoto H. & Zhou, Y. 2005 Determination of flow configurations and fluid forces acting on two staggered circular cylinders of equal diameter in cross-flow. *J. Fluids Struct*. 21, 363-394.

Alam, M.M., Zhou, Y. & Wang, X.W., 2010a The wake of two side-by-side square cylinders. *J. Fluid Mech* 669, 432-471.

Alam, M.M., Zhou, Y., Zho, Z.M., Flamand, O. & Buojard, O. 2010b Classification of the tripped cylinder wake and bi-stable phenomenon. *Int. J. Heat and Fluid Flow* 31, 845-560.

Bearman, P.W. 1965 Investigation of flow behind a two-dimensional model with blunt trailing edge and fitted with splitter plates. *J. Fluid Mech.* 21, 241–255.

Bokaian, A. & Geoola, F. 1984a Proximity-induced galloping of two interfering circular cylinder. *J. Fluid Mech.* 146, 417-449.

Bokaian, A. & Geoola, F. 1984b Wake-induced galloping of two interfering circular cylinder. *J. Fluid Mech.* 146, 383-415.

Borazjani, I. & Sotiropoulos, F. 2009 Vortex-induced vibrations of two cylinders in tandem arrangement in the proximity–wake interference region. *J. Fluid Mech.* 621, 321-364.

Brika, D. & Laneville, A. 1999 The flow interaction between a stationery cylinder and a downstream flexible cylinder. *J.*

Fluids Struc. 13, 579-606.

Cooper, K.R. 1973 Wind tunnel and theoretical investigations into the aerodynamic instability of smooth and stranded twin bundles power conductors. National Aeronautical Establishment Report LTR-LA-115, Ottawa, Canada.

Gu, Z. & Sun, T. 1999 On interference between two circular cylinders in staggered arrangement at high subcritical Reynolds numbers. *J. Wind Engng Indust. Aerodyn.* 80, 287–309.

Gursul, I. & Rockwell, D. 1990 Vortex-street impinging upon an elliptical leading edge. *J. Fluid Mech.* 211, 211–242.

Igarashi, T. 1984 Characteristics of the flow around two circular cylinders arranged in tandem (2nd Report). *Bull. the Japan Society of Mechanical Engineers* 27, 2380–2387.

Kim, S., Alam, M. M., Sakamoto, H. and Zhou, Y. 2009 Flow-induced vibrations of two circular cylinders in tandem arrangement, Part 1: characteristics of vibration. *J. Wind Engng Indust. Aerodyn.* 97, 304-311.

Kim, S., Takai, K., Sakamoto, H., Haniu, H. & Suzuki, S. 2008 Suppression and characteristics of flow-induced vibration of elastically supported two circular cylinders in side-by-side arrangement. *Transaction of the Japan Society of Mechanical Engineers* 74, No. 738, 337-344 (in Japanese).

King, R. & Johns, D.J. 1976 Wake interaction experiments with two flexible circular cylinders in flowing water. *J. Sound Vib.* 45, 259-283.

Knell, B.J. 1969 The drag of a circular cylinder fitted with shrouds. *Natl. Phys. Lab. (UK)*, Aero. Rep. no. 1297.

Lam, K.M. & To, A.P. 2003 Interference effect of an upstream larger cylinder on the lock-in vibration of a flexibly mounted circular cylinder. *J. Fluids Struc.17*, 1059-1078.

Meneghini, J.R., Satara, F., Siqueira, C.L.R. & Ferrari, J.A. 2001 Numerical simulation of flow interference between two circular cylinders in tandem and side-by-side arrangements. *J. Fluids Struct*. 15, 327–350.

Peschard, I. & Le Gal, P. 1996 Coupled wakes of cylinders. Phy. *Review Letters* 77, 3122–3125.

Price, J. 1976 The origin and nature of the lift force on the leeward of two bluff bodies. *Aeronautical Quarterly* 26, 154–168.

Price, S.J. & Paidoussis, M.P. 1984 The aerodynamic forces acting on groups of two and three circular cylinders when subject to a cross-flow. *J. Wind Engng Indust. Aerodyn.* 17, 329-347.

Ruscheweyh, H.P. 1983. Aeroelastic interference effects between slender structures. *J. Wind Eng. Ind. Aerodyn.* 14, 129-140.

Sakamoto, H., Takeuchi, N., Haniu, H. & Tan, K. 1997 Suppression of fluid forces acting on square prism by passive control. *J. Fluids Eng.* 119, 506–511.

Sumner D., Price, S.J. & Paidoussis, M.P. 2000 Flow-pattern identification for two staggered circular cylinders in cross-flow. *J. Fluid Mech.* 411, 263-303.

Wardlaw, R.L. & Cooper, K.R. 1973 A wind tunnel investigation of the steady aerodynamic forces on smooth and stranded twin bundled power conductors for the Aluminum Company of America. National Research Council of Canada, LTR-LA-117

Williamson, C.H.K and Roshko, A. 1988 Vortex formation in the wake of an oscillating cylinder. *J. Fluids Struc.* 2, 355-381.

Williamson, C.H.K. 1985 Evolution of a single wake behind a pair of bluff bodies. *J. Fluid Mech.* 159, 1–18.

Williamson, C.H.K. and Goverdhan, R. 2004 Vortex-induced vibrations. *Ann. Rev. Fluid Mech.* 36, 413-455.

Williamson, C.H.K., 1996. Three dimensional wake transition. *J. Fluid Mech.* 328, 345-407.

Zdravkovich, M.M. & Pridden, D.L. 1977 Interference between two circular cylinders; series of unexpected discontinuities. *J. Indust. Aerodyn*. 2, 255-270.

Zdravkovich, M.M. 1981 Review and classification of various aerodynamic and hydrodynamic means for suppressing vortex shedding. *J. Wind Engng Indust. Aerodyn.* 7, 145–189.

Zdravkovich, M.M. 1987 The effects of interference between circular cylinders in cross flow. *J. Fluids Struct*. 1, 239-261.